# Variational Graph Generator for Multi-View Graph Clustering

Jianpeng Chen,<sup>1</sup> Yawen Ling,<sup>1</sup> Jie Xu,<sup>1</sup> Yazhou Ren,<sup>1\*</sup> Shudong Huang,<sup>2</sup> Xiaorong Pu,<sup>1</sup> Lifang He<sup>3</sup>

<sup>1</sup>School of Computer Science and Engineering, University of Electronic Science and Technology of China, Chengdu, China,

<sup>2</sup>College of Computer Science, Sichuan University, Chengdu, China,

<sup>3</sup>Department of Computer Science and Engineering, Lehigh University, PA, USA

{cjpcool, yawen.Ling, jiexuwork}@outlook.com, {yazhou.ren, puxiaor}@uestc.edu.cn, huangsd@scu.edu.cn,

lih319@lehigh.edu

#### **Abstract**

Multi-view graph clustering (MGC) methods are increasingly being studied due to the rising of multi-view data with graph structural information. The critical point of MGC is to better utilize the view-specific and view-common information in features and graphs of multiple views. However, existing works have an inherent limitation that they are unable to concurrently utilize the consensus graph information across multiple graphs and the view-specific feature information. To address this issue, we propose Variational Graph Generator for Multi-View Graph Clustering (VGMGC). Specifically, a novel variational graph generator is proposed to infer a reliable variational consensus graph based on a priori assumption over multiple graphs. Then a simple yet effective graph encoder in conjunction with the multi-view clustering objective is presented to learn the desired graph embeddings for clustering, which embeds the consensus and view-specific graphs together with features. Finally, theoretical results illustrate the rationality of VGMGC by analyzing the uncertainty of the inferred consensus graph with information bottleneck principle. Extensive experiments demonstrate the superior performance of our VGMGC over SOTAs.

### 1 Intorduction

Attributed graph clustering has received increasing attention with the development of graph structure data, such as social networks, academic networks, and world wide web (Zhang et al. 2019; Velickovic et al. 2019; Wu et al. 2019). Attributed graph clustering aims to better analyze the graphs with its attributed features for clustering task, which can benefit lots of fields such as product recommendation and community detection. On the other hand, many of graph structure data contain multiple views in real-world applications, for example, graphs in social networks can be constructed based on common interests or followers of users, and graphs in academic networks can be established by co-authors or citations of papers. Therefore, lots of multiview graph clustering (MGC) methods have emerged in recent years for better mining the information of multi-view graphs (Nie, Li, and Li 2017; Cheng et al. 2020; Fan et al. 2020).

Generally, MGC methods could be categorized into two types (Nie, Li, and Li 2017; Fan et al. 2020). One type gen-

erates a global affinity matrix of all samples for all views and then clusters it into different classes (Nie, Li, and Li 2017; Xia et al. 2014; Wang, Yang, and Liu 2020). These methods successfully demonstrate the effectiveness of learning a consensus graph for analyzing all views. Another type learns representations for individual views via graph embedding techniques, and then incorporates them into global representations. Subsequently, traditional clustering methods, such as k-means (Macqueen 1967), can be adopted to obtain clustering results (Cheng et al. 2020). Benefitting from the graph embedding ability of Graph Neural Networks (GNNs) (Wu et al. 2019: Kipf and Welling 2017: Veličković et al. 2018; Zhu and Koniusz 2021), the two types of methods have been largely improved (Cheng et al. 2020; Fan et al. 2020; Pan and Kang 2021; Lin and Kang 2021). Nevertheless, both studies have inherent limitations. For the first type of works, the consensus graph reflects the common topological information of all views. But if we directly partition the consensus graph, the latent view-specific information in features will be ignored. As for the second type of works. each view's graph embeddings are learned separately, so the global topological information might be ignored. Therefore, can we develop a method that is able to assimilate both the view-common and view-specific topological information, to reserve more feature information as well as utilize the superior graph embedding ability of GNNs?

To achieve the above goal, we will have two major challenges: 1) how to explore the consensus information and utilize it to generate a consensus graph that is applicable to GNNs, and 2) how to design a GNN that could embed the view-specific information and the generated consensus graph into features together. Considering the first issue, the generated consensus graph requires some properties. First, it must imply the common information from both features and graphs. Second, if there is an observed graph that is unreliable, it should depend less on this unreliable graph, in other words, different graphs have different probabilities to be selected to generate the consensus graph. This property requires that we infer it with probability. Third, it should be sparse to avoid large storage and computation consumption, and meanwhile to improve the robustness (Zheng et al. 2020; Morris and Mutzel 2020). Considering on these properties, the technique of variational inference is a perfect match, which could infer sparse and discrete variables with prob-

<sup>\*</sup>Corresponding author.

ability. So, we first propose a priori assumption over multigraphs, and then implement a variational graph generator to infer a sparse consensus graph from global features based on this priori assumption (see Section 3.2). As to the second issue, the previous researches about GNNs (Wu et al. 2019; Morris and Mutzel 2020; Xu et al. 2019) have suggested that lots of parameters in GNNs are redundant, and the main representation ability of them comes from the message passing process. To this end, we design a simple yet effective encoder with a parameter-free message-passing method to embed the view-specific and view-common graph information together (see Section 3.3). In addition, we introduce our multi-view fusion method to incorporate all views' graph embeddings for clustering. Finally, our objective functions are proposed to optimize the model for the multi-view clustering task. For brevity, we call the proposed approach VG-MGC (Variational Graph Generator for Multi-View Graph Clustering). Furthermore, we have theoretically analyzed the rationality of generated graph, and empirically demonstrated the effectiveness of VGMGC. The contributions of this work include:

- We propose a novel variational graph generator based on a priori assumption over multi-graphs, which can generate a variational consensus graph with the required properties from global features for GNNs. To the best of our knowledge, this work is the first trial utilizing variational inference to infer a discrete graph for multi-view graph learning.
- We propose a simple yet effective encoder to embed the consensus graph and view-specific graphs into features, in a parameter-free message-passing manner.
- Theoretical analysis illustrates the rationality of the inferred consensus graph and our proposals. Experiments on four widely-used multi-view graph datasets demonstrate the superior performance of our method compared with SOTAs.

### 2 Related Works

Kingma and Welling (2014) proposed variational autoencoders (VAE), which has subsequently influenced lots of fields. For example, Dilokthanakul et al. (2016) introduced VAE for clustering task. Xu et al. (2021b) disentangled view-specific and view-common information via VAE for multi-view clustering task. In the field of graph clustering, Kipf and Welling (2016) first adopted this technique to graph representation learning for link prediction. Following this work, Pan et al. (2018) proposed a variational adversarial approach to learn a robust graph embedding. Sun et al. (2021) extended graph VAE to infer stochastic node representations. However, all these works aim at inferring the node representations rather than a graph.

It seems hard to utilize variation to infer a graph since the observed graph is certain and prior distribution of the graph is unknown. Even so, a few works have still tried to infer a graph. Luo et al. (2020) introduced prior to graph, and sampled a new graph from observed one via uniform distribution. However, this graph is only a subgraph of the observed graph. Elinas, Bonilla, and Tiao (2020) introduced two hyper-parameters to control the uncertainty of a graph, and generated a graph based on variational inference and k-nearest neighbors (KNN). But it also faces two substantial issues. First, the selection of the two hyper-parameters is groundless. Second, its variational ability is largely restricted by KNN, and the k in KNN is hard to set. Differently, in the proposed variational graph generator, the uncertainty is dependent on how reliable the observed graphs are for the clustering task. Therefore, the inferred graph is more robust and task-related. Moreover, to the best of our knowledge, this is the first trial to infer a graph for multi-view clustering task.

# 3 Methods

**Problem Statement** Given multiple graphs with their attributed features  $\{\mathcal{G}^v = (\mathbf{X}^v, \mathbf{A}^v)\}_{v=1}^V$ , where  $\mathbf{X}^v \in \mathbb{R}^{n \times d_v}$  denotes the features of n samples and  $\mathbf{A}^v = \{a_{ij} \mid a_{ij} \in \{0,1\}\}$  denotes the adjacent matrix (with self-loop) of the v-th view, respectively, MGC aims to partition the n samples into c classes. Letting a diagonal matrix  $\mathbf{D}^v$  (where  $\mathbf{D}^v_{ii} = \sum_j a^v_{ij}$ ) represent the degree matrix of  $\mathbf{A}^v$ , the normalized adjacent matrix is defined as  $\widetilde{\mathbf{A}}^v = (\mathbf{D}^v)^{-1}\mathbf{A}^v$ . We define  $\overline{\mathbf{X}} \in \mathbb{R}^{n \times d'}$  as a global feature shared by all views. Generally, if the dataset does not contain this feature, it is generated by concatenating  $\{\mathbf{X}^v\}_{v=1}^V$ , i.e.,  $\overline{\mathbf{X}} = Concat(\mathbf{X}^1, \mathbf{X}^2, ..., \mathbf{X}^V)$  where  $Concat(\cdot, \cdot)$  denotes concatenating operation. Specifically, let  $\overline{\mathbf{Z}} \in \mathbb{R}^{n \times (V \cdot D)}$  and  $\mathbf{Z}^v \in \mathbb{R}^{n \times D}$  be the global and each view's latent representation respectively. The goal of this work is to learn better MGC by leveraging the novel variational graph generator and an effective graph encoder. The overall descriptions of notations are shown in Appendix A.

## 3.1 Overview of Variational Graph Generator for Multi-View Graph Clustering

The overview of VGMGC is shown in Figure 1. In the following, we will concentrate on three questions to disassemble our proposed framework: a) how the variational consensus graph is inferred from multi-view graph data (see Section 3.2), b) how the variational consensus graph is incorporated with each view's specific graph and features to generate latent feature  $\mathbf{Z}^v$  (see Section 3.3), and c) how to fuse multi-view latent features for collaborative training and clustering (see Section 3.4).

### 3.2 Variational Graph Generator

We first present our variational graph generator, which infers a discrete latent graph from the global features  $\overline{\mathbf{X}}$ . The main difference between the variational graph generator and previous VAEs (Kingma and Welling 2014; Dilokthanakul et al. 2016; Xu et al. 2021b; Kipf and Welling 2016) is that we aim at inferring a discrete graph but not embeddings, and our task-related priori assumption over multi-graphs is novel.

Let  $\hat{\mathbf{S}} = \{\hat{s}_{ij} \mid \hat{s}_{ij} \in \{0,1\}\}$  be an independent consensus graph, we aim to model the multi-graph data  $\{\mathbf{A}^v\}_{v=1}^V$  to find a better consensus graph. Therefore, this generative

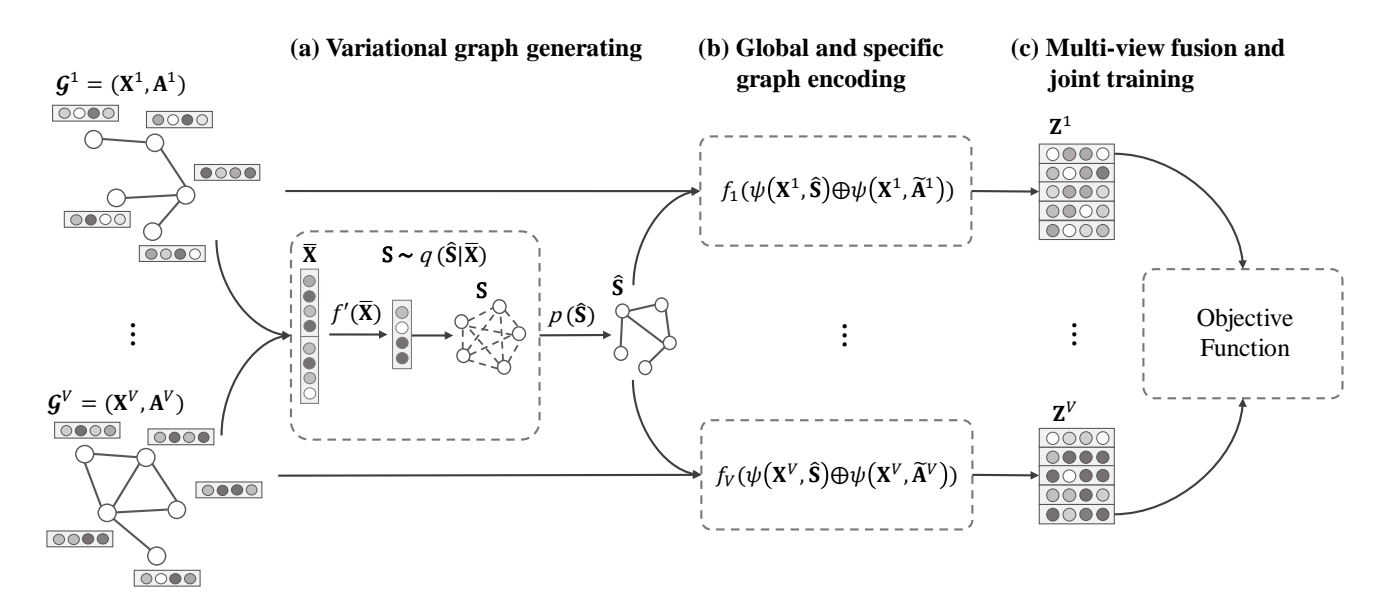


Figure 1: The illustration of VGMGC.  $\oplus$  denotes concatenating operation. We first infer a cross-view consensus graph  $\hat{\mathbf{S}}$  via the variational graph generator, and then, the variational consensus graph is normalized, and we feed it with each attributed view-specific graph into the graph encoder, which could generate latent features  $\mathbf{Z}^v$  for each view. Finally, all views' latent features are weighted and concatenated for training or clustering.

model could be written as:

$$p(\mathbf{X}^v, \hat{\mathbf{S}}, \mathbf{A}^v) = p(\mathbf{A}^v \mid \mathbf{X}^v, \hat{\mathbf{S}}) p(\mathbf{X}^v, \hat{\mathbf{S}}), \tag{1}$$

where  $p(\cdot)$  represents the probability.

**Priori Assumption over Multi-Graph** We consider that the consensus graph is a Gilbert random graph (Gilbert 1959), where the edges in  $\hat{\mathbf{S}}$  are conditionally independent with each other, so the probability of generating  $\hat{\mathbf{S}}$  could be factorized as:

$$p(\hat{\mathbf{S}}) = \prod_{i,j} p(\hat{s}_{ij}). \tag{2}$$

An evident instantiation of  $p(\hat{s}_{ij})$  is the Bernoulli distribution, i.e.,  $\hat{s}_{ij} \sim Bern(\beta_{ij}).$   $p(\hat{s}_{ij}=1)=\beta_{ij}$  is the prior probability of whether there exists a edge between node i and j, where  $\beta$  are parameters determined by all observed graphs  $\{\mathbf{A}^v\}$  with their corresponding optimizable beliefs  $\{b^v\}$ . The belief  $b^v \in (0,1]$  of  $\mathbf{A}^v$ , which could be obtained by a self-supervised method (which will be introduced in Section 3.4), is to control how much the v-th graph should be trusted for our clustering task. Then, we aggregate all graphs  $\{\mathbf{A}^v\}$  with their corresponding beliefs  $\{b^v\}$  to obtain the priori parameter  $\beta$ :

$$\beta_{ij} = \frac{\sum_{v} [b^{v} \cdot a_{ij}^{v} + (1 - b^{v}) \cdot (1 - a_{ij}^{v})]}{\sum_{v} b^{v}}.$$
 (3)

**Inference Process** The variational consensus graph  $\hat{\mathbf{S}}$  is generated from global features  $\overline{\mathbf{X}}$ , so the posterior of  $\hat{\mathbf{S}}$  could be written as  $p(\hat{\mathbf{S}} \mid \overline{\mathbf{X}})$ . However, considering the posterior is intractable to be calculated (Kingma and Welling 2014; Dilokthanakul et al. 2016), we propose a neural network

which is based on self-attention (Vaswani et al. 2017) to approximate it, *i.e.*,  $q_{\phi'}(\hat{\mathbf{S}} \mid \overline{\mathbf{X}})$  where  $\phi'$  denotes the trainable parameters of the neural network. The proposed neural network could be written as:

$$\alpha = \mathbf{K}\mathbf{Q}^T$$
, where  $\mathbf{K} = f'(\overline{\mathbf{X}}), \mathbf{Q} = \mathbf{K}\mathbf{W}$ , (4)

where  $\alpha = \{\alpha_{ij}\} \in \mathbb{R}^{n \times n}$  denotes the neurons used to obtain variable  $\hat{\mathbf{S}}$ , f' represents a multilayer perceptron (MLP), and  $\mathbf{W}$  is the trainable parameters. Therefore,  $\phi'$  contains trainable parameters in f' and  $\mathbf{W}$ . Because the structural information  $\alpha$  needs to reserve the important information of global features  $\overline{\mathbf{X}}$ . In doing so, we maximize the mutual information between  $\alpha$  and  $\overline{\mathbf{X}}$ :

$$\max_{\phi'} I(\alpha, \overline{\mathbf{X}}) = \max_{\phi'} I(\mathbf{Q}, \overline{\mathbf{X}}). \tag{5}$$

Moreover, due to the discrete nature of graph  $\hat{\mathbf{S}}$ , we adopt reparameterization trick to optimize these parameters with gradient-based methods (Jang, Gu, and Poole 2016). In this work we utilize binary concrete distribution (Maddison, Mnih, and Teh 2016) for relaxation, i.e.,  $s_{ij} \sim BinConcrete(\alpha_{ij},\tau)$ , where  $\tau>0$  and  $\alpha_{ij}$  represent the temperature and location parameters respectively. Specifically, let variable  $U \sim Uniform(0,1)$ , the relaxed weight  $s_{ij} \in (0,1)$  of edge (i,j) is calculated as:

$$q_{\phi'}(\hat{s}_{ij} \mid \overline{\mathbf{x}}) = \sigma((\log U - \log(1 - U) + \alpha_{ij})/\tau),$$
  
with  $U \sim Uniform(0, 1),$  (6)

where  $\sigma(\cdot)$  denotes the *Sigmoid* function. It is easy to demonstrate the rationality of using the binary concrete distribution of  $s_{ij}$  to approximate the priori Bernoulli distribution of  $\hat{s}_{ij}$ .

**Generative Process** After obtaining the latent consensus graph  $\hat{\mathbf{S}}$ , in the generative process, we model all views' graphs  $\{\mathbf{A}^v\}_{v=1}^V$  in a collaborative manner. Let  $\{\xi^v\}$  be the learnable parameters of decoder, the likelihood of v-th graph is as follow:

$$\check{\mathbf{A}}^v = p_{\xi^v}(\mathbf{A}^v \mid \hat{\mathbf{S}}, \mathbf{X}^v). \tag{7}$$

**Evidence Lower Bound** According to Jensen's inequality, it is easy to prove that maximizing the likelihood of observed graphs (*i.e.*,  $p(\mathbf{A}^v)$ ) is equal to maximizing the evidence lower bound (ELBO):

$$\max_{\phi', \{\xi^v\}_{v=1}^V} \mathcal{L}_E = \sum_{v=1}^V \mathbb{E}_{q_{\phi'}(\widehat{\mathbf{S}}|\overline{\mathbf{X}})} \left[ \log p_{\xi^v}(\mathbf{A}^v \mid \widehat{\mathbf{S}}, \mathbf{X}^v) \right] - KL \left( q_{\phi'}(\widehat{\mathbf{S}} \mid \overline{\mathbf{X}}) \parallel p(\widehat{\mathbf{S}}) \right).$$
(8)

The first term of Eq. (8) is the expectation of the conditional likelihood over the approximate posterior, *i.e.*, expected log likelihood (ELL), and the second term is the KL divergence between the approximate posterior of the variational consensus graph and its prior. Under our priori assumption, *i.e.*,  $p(s_{ij}) = Bern(\beta_{ij})$ , the KL divergence is bounded:

$$KL\left(q_{\phi'}(\hat{\mathbf{S}} \mid \overline{\mathbf{X}}) \parallel p(\hat{\mathbf{S}})\right) = -H(q_{\phi'}(\hat{\mathbf{S}})) + \sum_{ij} \log \frac{1}{\beta_{ij}}$$

$$\leq \sum_{ij} \log \frac{1}{\beta_{ij}},$$
(9)

where  $H(\cdot)$  denotes Entropy and  $\beta$  is determined by the observed graphs and corresponding beliefs (see Eq. (3)). Therefore, the maximum variational information in the variational consensus graph is dependent on the consistency of these observed graphs and how relative they are to our clustering task. Specifically, when all graphs are consistent with  $\{a_{ij}^v=1\}_{v=1}^V$ , we could get  $\log\beta_{ij}=1$ , which enforces  $H(q(\hat{s}_{ij}))=0$ .

### 3.3 Global and Specific Graph Encoding

In this section, we will propose our graph encoder, which contains three inputs, *i.e.*, observed graph data  $\mathbf{A}^v$  with its attributed features  $\mathbf{X}^v$ , and a variational consensus graph  $\hat{\mathbf{S}}$ . The aim of this graph encoder is to inject the consensus graph structure information into each specific view and generate embeddings. So this module could be decomposed to two steps: 1) message-passing-based graph embedding (denoted by  $\psi(\cdot)$ ) to embed the specific and consensus graph structure respectively; 2) low-dimensional representation learning (denoted by  $f_v(\cdot)$ ) to fuse the view-specific graph embeddings and consensus graph embeddings while obtaining a lower-dimensional representations.

**Message-Passing-Based Graph Embedding** Inspired by previous GNNs (Wu et al. 2019; Zhu and Koniusz 2021; Chen et al. 2020), we remove most redundant parameters in GNNs and introduce a simple yet effective message-passing method:

$$\psi(\mathbf{X}, \widetilde{\mathbf{A}}) = \left(\sum_{l=0}^{order} \widetilde{\mathbf{A}}^l + \mathbf{I}\right) \mathbf{X},\tag{10}$$

where order is a hyper-parameter which denotes the aggregation orders on graph  $\mathbf{A}$ , and  $\mathbf{I}$  denotes the identity matrix.  $\widetilde{\mathbf{A}}$  and  $\mathbf{X}$  are normalized graphs with their attributed features. The intuitions behind Eq. (10) are stated in Appendix D.

**Low-Dimensional Representation** A straightforward instantiation of  $f_v(\widetilde{\mathbf{A}}, \widehat{\mathbf{S}}, \mathbf{X})$  is MLP. Concretely, we concatenate the specific graph embeddings and consensus graph embeddings and feed them into this MLP to get a lower-dimensional embeddings  $\mathbf{Z}^v \in \mathbb{R}^{n \times D}$ :

$$\mathbf{Z}^{v} = f_{v}(\widetilde{\mathbf{A}}^{v}, \widehat{\mathbf{S}}, \mathbf{X}^{v})$$

$$= f_{v}\left(Concat(\psi(\mathbf{X}^{v}, \widetilde{\mathbf{A}}^{v}), \psi(\mathbf{X}^{v}, \widehat{\mathbf{S}}))\right),$$
(11)

Here, the propagation of  $\mathbf{X}^v$  over  $\psi$  and  $f_v$  will lead to some information loss. To reserve more view-specific feature information, we maximize the mutual information  $I(\mathbf{X}^v, \mathbf{Z}^v)$ :

$$\max_{\phi^v} I(\mathbf{Z}^v, \mathbf{X}^v), \tag{12}$$

where  $\phi^v$  represents the learnable parameters in  $f_v$ .

## 3.4 Multi-View Fusion for Clustering Task

**Multi-View Fusion** To fuse all views' embeddings  $\{\mathbf{Z}^v\}_{v=1}^V$ , we first assign beliefs  $\{b^v\}_{v=1}^V$  to every view. Intuitively, these beliefs indicate how the corresponding view is relative to our clustering task. Then, we reweight every view via its belief, and concatenate them to get final global representations  $\overline{\mathbf{Z}} \in \mathbb{R}^{n \times (V \cdot D)}$ . This process could be formulated as:

$$\overline{\mathbf{Z}} = Concat(b^1 \mathbf{Z}^1, b^2 \mathbf{Z}^2, ..., b^V \mathbf{Z}^V). \tag{13}$$

This global representation  $\{\mathbf{Z}^v\}_{v=1}^V$  is then fed into k-means for clustering. Therefore, how to find correct belief for each view is crucial. To this end, we propose a self-supervised strategy. We first initialize all beliefs to 1, *i.e.*,  $\{b^{(0),v}=1\}^V$ , then, we generate  $\overline{\mathbf{Z}}^{(t-1)}$  via Eq. (13) and conduct k-means on it to obtain the pseudo-labels of t-th epoch. Meanwhile, each view's predicted labels are also obtained by k-means. After that, we consider the pseudo-labels from  $\overline{\mathbf{Z}}^{(t-1)}$  as ground-truth and other predicted labels from  $\{\mathbf{Z}^v\}^V$  as prediction results to compute each view's clustering score (like normalized mutual information), i.e.,  $score^{(t),v}$ . These scores are normalized for updating beliefs:

$$b^{(t),v} = \left(\frac{score^{(t),v}}{\max(score^{(t),1}, score^{(t),2}, \dots, score^{(t),V})}\right)^{\rho}, \tag{14}$$

where  $\rho \geq 0$  is a soft parameter. When  $\rho = 0$ , we can get  $b^{(t),v} = 1$  for all t and v, which denotes that all graphs are equally believed; when  $\rho \to \infty$ ,  $\{b^{(t),v}\}$  are binarized. Finally, we can generate  $\overline{\mathbf{Z}}^{(t)}$  via Eq. (13) under the new beliefs  $\{b^{(t),v}\}$ , which will be utilized to train the model and generate a more correct belief in next epoch.

**Multi-View Clustering Loss** The clustering loss is widely used in traditional clustering task (Cheng et al. 2020; Xie, Girshick, and Farhadi 2016; Xu et al. 2021a), which encourages the assignment distribution of samples in the same cluster being more similar. Concretely, let  $Q^v$  be a soft assignment calculated by Student's t-distribution (Maaten and Hinton 2008) of v-th view, and  $P^v$  be a target distribution calculated by sharpening the soft assignment  $Q^v$ . For MGC, we encourage each view's soft distribution to fit the global representation's target distribution by KL divergence:

$$\mathcal{L}_c = \sum_{v=1}^{V} KL(\overline{P} \| Q^v) + KL(\overline{P} \| \overline{Q}), \tag{15}$$

where  $\overline{P}$  and  $\overline{Q}$  denote the target and soft distribution of global representation  $\overline{\mathbf{Z}}$ .

### 3.5 Objective Function

Our objective function contains three parts: maximizing ELBO  $(\mathcal{L}_E)$  to optimize the variational graph generator; maximizing mutual information  $(I(\mathbf{Z}^v, \mathbf{X}^v))$  and  $I(\mathbf{Q}, \overline{\mathbf{X}})$  to reserve feature information; and minimizing clustering loss  $(\mathcal{L}_c)$  to optimize the task-related clustering results.  $\gamma_c$  and  $\gamma_E$  are introduced to trade off the numerical value of  $\mathcal{L}_c$  and  $\mathcal{L}_E$ . Formally, we have the objective function:

$$\min_{\phi',\eta',\{\phi^v\},\{\eta^v\}} \mathcal{L}_r + \gamma_c \mathcal{L}_c - \gamma_E \mathcal{L}_E.$$
 (16)

Here,  $\mathcal{L}_r$  is an instantiation of negative lower bound of  $I(\mathbf{Z}^v, \mathbf{X}^v)$  and  $I(\boldsymbol{\alpha}, \overline{\mathbf{X}})$  (see Section 3.6), and  $\{\eta^v\}$  and  $\eta'$  denote corresponding learnable parameters. Notably, the parameters of  $p_{\xi^v}(\mathbf{A}^v \mid \hat{\mathbf{S}}, \mathbf{X}^v)$  and  $f_v$  are shared in our model, so  $\{\xi^v\}$  is omitted in Eq. (16).

### 3.6 Theoretical Analysis

Uncertainty of Consensus Graph Let  $H(\hat{\mathbf{S}})$  denote the uncertainty of  $\hat{\mathbf{S}}$ , and  $d_{Ham}(\mathbf{A}^1, \mathbf{A}^2)$  denote the Hamming distance, which quantizes the inconsistency of graph  $\mathbf{A}^1$  and  $\mathbf{A}^2$ . We have the following proposition:

**Proposition 1.** Assume all graphs are equally reliable, the more consistent the observed graphs are, the less uncertain the consensus graph is, and vice versa:

$$H(\hat{\mathbf{S}}) \propto d_{Ham}(\mathbf{A}^1, \mathbf{A}^2).$$
 (17)

Using  $H(\mathbf{A}^v, \hat{\mathbf{S}})$  (e.g., cross entropy) to depict the similarity between the distribution of  $\hat{\mathbf{S}}$  and  $\mathbf{A}^v$ , and the belief  $b^v \in (0,1]$  can represent the relevance of v-th view to our clustering task, we have:

**Proposition 2.** For a specific graph, the more this graph relative to the clustering task, the more the distribution of  $\hat{\mathbf{S}}$  similar to it, and vice versa:

$$H(\mathbf{A}^v, \mathbf{\hat{S}}) \propto b^v.$$
 (18)

From the two propositions, we can conclude the following theorem:

**Theorem 1.** The distribution of  $\hat{\mathbf{S}}$  is dependent on the consistency of observed graphs and how much they are related to the clustering task.

**Information Bottleneck Principle of Variational Graph Generator** To understand how the variational graph generator infers a graph with sufficient information, we build a connection between the objective function of the variational graph generator (Section 3.2) and Information Bottleneck (IB) principle (Alemi et al. 2017; Amjad and Geiger 2020). Recall the definition of supervised IB (Tishby, Pereira, and Bialek 2000):

**Definition 1.** The supervised IB is to maximize the Information Bottleneck Lagrangian:

$$\mathcal{IB}_{sup} = I(Y, Z_X) - \omega I(X, Z_X), \text{ where } \omega > 0.$$
 (19)

This shows that the supervised IB aims to maximize the mutual information between latent representation  $Z_X$  and corresponding target labels Y, meanwhile trying to compress more information from X (i.e., minimize the mutual information between X and  $Z_X$ ). The intuition behind IB is that the latent variable  $Z_X$  tries to collect less but sufficient information from X to facilitate the task.

Recall the proposed method, VGMGC aims at inferring the graph  $\hat{\mathbf{S}}$  from global features  $\overline{\mathbf{X}}$  in the inference process, and generating the observed graphs  $\mathbf{A}^v$  in the generative process. Intuitively, only the topological information in  $\overline{\mathbf{X}}$  is useful and most others are redundant. Therefore, we have the following variational IB:

**Definition 2.** The IB in variational graph generator is:

$$\mathcal{IB}_{var} = \sum_{v} I(\mathbf{A}^{v}, \hat{\mathbf{S}}) - \omega I(\hat{\mathbf{S}}, \overline{\mathbf{X}}), \text{ where } \omega > 0.$$
 (20)

**Theorem 2.** Maximizing the ELBO (Eq. (8)) is equivalent to maximizing IB when  $\omega = 1$ :

$$\max \mathcal{L}_E \cong \max \mathcal{IB}_{var}. \tag{21}$$

Eq (21) indicates that by optimizing Eq. (8), the consensus graph  $\hat{\mathbf{S}}$  can capture the most useful topological information and discard redundant information from global feature  $\overline{\mathbf{X}}$ .

**Lower Bound of Mutual Information** We analyze the lower bound of mutual information for optimizing  $I(\mathbf{Z}^v, \mathbf{X}^v)$  and  $I(\boldsymbol{\alpha}^v, \overline{\mathbf{X}})$ .

**Definition 3.** The mutual information  $I(\mathbf{Z}^v, \mathbf{X}^v)$  is:

$$I(\mathbf{Z}^{v}, \mathbf{X}^{v}) = \mathbb{E}_{p(\mathbf{z}^{v}, \mathbf{x}^{v})} \log \frac{p(\mathbf{z}^{v}, \mathbf{x}^{v})}{p(\mathbf{z}^{v})p(\mathbf{x}^{v})}$$

$$= \mathbb{E}_{p(\mathbf{z}^{v}, \mathbf{x}^{v})} \log p(\mathbf{x}^{v} \mid \mathbf{z}^{v}) + H(\mathbf{x}^{v}).$$
(22)

In Eq. (22), considering  $p(\mathbf{x}^v \mid \mathbf{z}^v)$  is intractable, so  $q_{\eta^v}(\mathbf{x}^v \mid \mathbf{z}^v)$  is introduced as a variational approximation of  $p(\mathbf{x}^v \mid \mathbf{z}^v)$ . After that, we can obtain the lower bound of mutual information:

**Theorem 3.** *Maximizing mutual information is equivalent to maximizing its lower bound:* 

$$\max I(\mathbf{Z}^v, \mathbf{X}^v) \cong \max \mathbb{E}_{q_{\eta^v}(\mathbf{x}^v \mid \mathbf{z}^v)} \log q_{\eta^v}(\mathbf{x}^v \mid \mathbf{z}^v). \tag{23}$$

In our case,  $x_j^v$  is subordinated to Bernoulli distribution, so  $-\mathbb{E}_{p(\mathbf{z}^v|\mathbf{x}^v)p(\mathbf{x}^v)}\log q_{\eta^v}(\mathbf{x}^v\mid\mathbf{z}^v)$  can be instantiated by a binary cross entropy loss between  $\mathbf{x}^v$  and its reconstruction  $\breve{\mathbf{x}}^v$ . The lower bound of all  $I(\mathbf{Z}^v,\mathbf{X}^v)$  and  $I(\alpha,\overline{\mathbf{X}})$  are added together, written as  $\mathcal{L}_r$ .

Methods / Datasets	Amazon photos NMI% ARI% ACC% F1%			NMI%	Amazon c ARI%	omputers ACC%	F1%		
MAGCN (Cheng et al. 2020)	39.0	24.0	51.7	47.3	-	_	_	_	
COMPLETER (Lin et al. 2021)	26.1	7.6	36.8	30.7	15.6	5.4	24.2	16.0	
MVGRL (Lin et al. 2021)	43.3	23.8	50.5	46.0	10.1	5.5	24.5	17.1	
MvAGC (Lin and Kang 2021)	52.4	39.7	67.8	64.0	39.6	32.2	58.0	41.2	
MCGC (Pan and Kang 2021)	61.5	43.2	71.6	68.6	53.2	39.0	59.7	52.0	
VGMGC	66.8	58.4	78.5	76.9	53.5	47.5	62.2	50.2	
Methods / Datasets		AC	M			DBLP			
RMSC (Xia et al. 2014)	39.7	33.1	63.2	57.5	71.1	76.5	89.9	82.5	
LINE (Tang et al. 2015)	39.4	34.3	64.8	65.9	66.8	69.9	86.9	85.5	
GAE (Kipf and Welling 2016)	49.1	54.4	82.2	82.3	69.3	74.1	88.6	87.4	
PMNE (Liu et al. 2017)	46.5	43.0	69.4	69.6	59.1	52.7	79.3	79.7	
SwMC (Nie et al. 2017)	8.4	4.0	41.6	47.1	37.6	38.0	65.4	56.0	
MNE (Zhan et al. 2018)	30.0	24.9	63.7	64.8	_	_	_	_	
O2MAC (Fan et al. 2020)	69.2	73.9	90.4	90.5	72.9	77.8	90.7	90.1	
MvAGC (Lin and Kang 2021)	67.4	72.1	89.8	89.9	77.2	82.8	92.8	92.3	
MCGC (Pan and Kang 2021)	71.3	76.3	91.5	91.6	83.0	77.5	93.0	92.5	
VGMGC	76.3	81.9	93.6	93.6	78.3	83.7	93.2	92.7	

Table 1: The overall clustering results. The best results are shown in bold, and the results which are not reported in the original papers are denoted by '-'.

## 4 Experiments

We conduct the experiments on four widely-used multigraph datasets (*i.e.* ACM, DBLP, Amazon photos and Amazon computers), and compare the proposed VGMGC with several baselines and SOTAs, including LINE (Tang et al. 2015), GAE (Kipf and Welling 2016), RMSC (Xia et al. 2014), PMNE (Liu et al. 2017), SwMC (Nie et al. 2017), MNE (Zhan et al. 2018), O2MAC (Fan et al. 2020), MAGCN (Cheng et al. 2020), MvAGC (Lin and Kang 2021), MCGC (Pan and Kang 2021), COMPLETER (Lin et al. 2021) and MVGRL (Hassani and Khasahmadi 2020). For the evaluation, normalized mutual information (NMI), adjusted rand index (ARI), accuracy (ACC) and F1-score (F1) are adopted. More details are presented in Appendix C.

### 4.1 Overall Results

Table 1 shows the clustering performance of the proposed VGMGC and comparison methods on four multi-graph datasets. Intuitively, VGMGC outperforms the best SOTA, *i.e.* MCGC, with ACC boosting 6.9%, 2.5%, 2.1% and 0.1% on the four different datasets respectively. Moreover, it shows an overwhelming advantage with respect to ACM and Amazon photos, improving NMI both by more than 5%. In all, with the help of the generated variational consensus graph, the proposed VGMGC achieves superior performance compared with the existing MGC SOTAs.

### 4.2 Generalization to Other Datasets

In this section, we explore how well VGMGC performed on other two types of datasets, *i.e.*, single-view graph dataset Cora and traditional multi-view dataset Three Sources. For comparison, we select several variational-based graph clustering methods including VGAE (Kipf and Welling 2016),

ARVGE (Pan et al. 2018) and GMM-VGAE (Binyuan, Pengfei, and Qinghua 2020), and some SOTAs including DNENC (Wang et al. 2022), MAGCN (Cheng et al. 2020), GMC (Wang, Yang, and Liu 2020), CGD (Tang et al. 2020) and SDSNE (Chenghua et al. 2022). More results can be found in Appendix E.

Table 2 compares the clustering results on the two types of datasets. It is clear that VGMGC performs best on both single-view graph dataset and traditional multi-view dataset compared with previous SOTAs. Specifically, we can see that the F1 score of VGMGC increases 3.4% on Cora and 2.9% on Three Sources compared to the previous SOTA, DNENC and SDSNE, respectively, which demonstrates that VGMGC can be well generalized to both single-view graph clustering and traditional multi-view clustering tasks.

### 4.3 Ablation Study

For simplicity, we present the ablation study results of VG-MGC on DBLP in this subsection, including the effect of each component and the performance on each single view. More details about the ablation study can be found in Appendix E.

Effect of Each Component As shown in the upper part of Table 3, without any of the components, the performance of VGMGC is negatively affected to varying degrees. Specifically, the generated consensus graph  $\hat{\mathbf{S}}$  plays an important role. Without the consensus graph and its guidance (see w/o  $\hat{\mathbf{S}}$  &  $\mathcal{L}_E$ ), the dramatic drop in performance demonstrates that the variational consensus graph  $\hat{\mathbf{S}}$  can mine enough global topological information.  $\mathcal{L}_T$  also makes a considerable contribution to the overall performance (see w/o  $\mathcal{L}_T$ ), as the  $\mathbf{Z}^v$  of specific view can preserve useful information from  $\mathbf{X}^v$ . Furthermore, this means the latent representations  $\overline{\mathbf{Z}}$  has

	1	Co	<b>**</b> 0	
Methods / Datasets	NMI%	Co ARI%	ra ACC%	F1%
VGAE (2016)	40.8	34.7	59.2	45.6
ARVGE (2018)	45.0	37.4	63.8	62.7
GMM-VGAE (2020)	54.4	_	71.5	67.8
MAGCN (2020)	55.3	47.6	71.0	_
DNENC (2022)	52.8	49.6	70.4	68.2
VGMGC	57.2	53.5	73.6	71.6
Methods / Datasets		Three S	ources	
GMC (2020)	54.8	44.3	69.2	60.5
CGD (2020)	69.5	61.1	78.1	70.9
O2MAC (2020)	72.7	75.5	65.0	66.9
SDSNE (2022)	84.8	86.7	93.5	89.8
VGMGC	85.9	87.6	94.1	92.7

Table 2: Clustering results on a single-view graph dataset Cora and a traditional multi-view dataset Three Sources. The best results are shown in bold, and '–' denotes the result which is not reported in the original paper.

	DBLP						
Components / Datasets	NMI%	ARI%	ACC%	F1%			
VGMGC (w/o $\mathcal{L}_c$ )	77.9	83.2	93.0	92.4			
VGMGC (w/o $\mathcal{L}_r$ )	76.2	81.4	92.1	91.3			
VGMGC (w/o $\hat{\mathbf{S}}$ & $\mathcal{L}_E$ )	20.7	17.8	47.1	44.8			
VGMGC-single ( $\mathcal{G}^1$ )	47.7	52.5	79.0	78.6			
VGMGC-single ( $\mathcal{G}^2$ )	75.8	80.9	91.9	91.0			
VGMGC-single ( $\mathcal{G}^3$ )	15.6	11.1	45.9	45.3			
VGMGC-original	78.3	83.7	93.2	92.7			

Table 3: The ablation study results of VGMGC on DBLP. The oringal results of VGMGC are shown in bold.

included enough clustering information. Thus, the clustering loss  $\mathcal{L}_c$  is helpful, while it seems to be faint (see w/o  $\mathcal{L}_c$ ).

**Performance on Each View** We run VGMGC on each single view to test how much effect VGMGC has gained from these multiple views helping with each other. The last three rows of Table 3 show the results (see VGMGC-single). As can be seen, the clustering results of the original VGMGC outperforms all other single views' methods. Specifically, the NMI of VGMGC increases 2.5% comparing to the best single-view results (VGMGC-single ( $\mathcal{G}^2$ )), which indicates that VGMGC can well leverage the information from different views to obtain better clustering results.

### 4.4 Analysis

**Oversmoothing Analyis** The left side of Figure 2 shows the performance with different orders. Overall, the ACC increases with the increase of order, which suggests that VGMGC can mitigate oversmoothing. Notably, the plot on DBLP is steady, a possible explanation for this might because that VGMGC has learnt sufficient clustering-related information from original features directly.

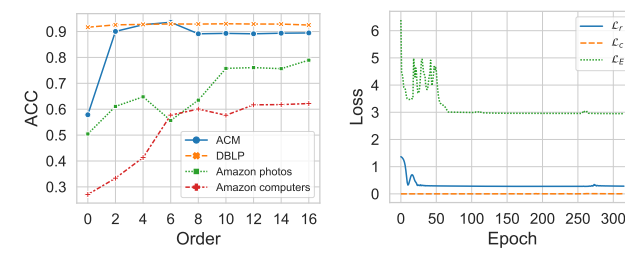


Figure 2: Left depicts the performance with different orders. Right depicts the training process on ACM.

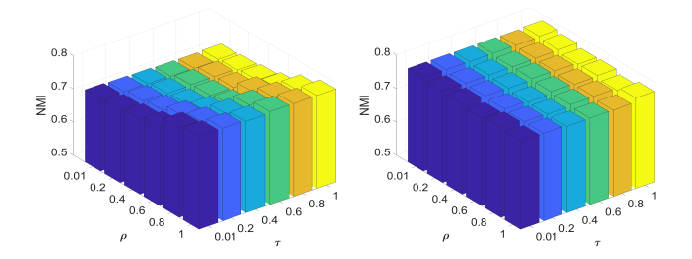


Figure 3: Sensitive analysis of NMI with  $\rho$  and  $\tau$  on ACM (left) and DBLP (right).

**Convergence Analysis** The right side of Figure 2 shows the trend of losses with training epochs. We can see that all losses converge after training around 100 epochs. Specifically, the value of  $\mathcal{L}_E$  is large and  $\mathcal{L}_c$  is relatively small.

Parameter Sensitive Analysis Figure 3 depicts how much the parameter  $\rho$  and  $\tau$  influence VGMGC. In general, the influences of both  $\rho$  and  $\tau$  are minor to VGMGC, and  $\rho$  is more influential than  $\tau$ . Notably, VGMGC has a more stable performance on DBLP. Specifically, it can be seen that NMI trends to increase on ACM but decrease on DBLP as the hyper-parameter  $\rho$  increases. We could speculate that the information from different views may be harmful on ACM but more compatible and helpful on DBLP. This is due to the fact that the  $\rho$  determines how much the bad view influence our model, as discussed in Section 3.4. VGMGC, on the other hand, behaves relatively stable for different values of  $\tau$  which impacts on the distribution of  $s_{ij}$ . More explorations about  $\tau$  are reported in Appendix E.

### 5 Conclusions

In this paper, we propose a multi-view graph clustering method to better mine and embed the consensus topological information of all graphs while reserving useful feature information, which is called variational graph generator for multi-view graph clustering (VGMGC). VGMGC can resolve the neglected inherent issues that existed in previous MGC works. We expect our work could inspire more researches, such as graph generation and multi-graph learning. The proposed method is limited to the clustering task, for other tasks it needs to change the score function to compute the belief of each graph.

### References

- Alemi, A. A.; Fischer, I.; Dillon, J. V.; and Murphy, K. 2017. Deep Variational Information Bottleneck. In *ICLR*.
- Amjad, R. A.; and Geiger, B. C. 2020. Learning Representations for Neural Network-Based Classification Using the Information Bottleneck Principle. *TPAMI*, 42(9): 2225–2239.
- Binyuan, H.; Pengfei, Z.; and Qinghua, H. 2020. Collaborative Graph Convolutional Networks: Unsupervised Learning Meets Semi-Supervised Learning. In *AAAI*.
- Chen, M.; Wei, Z.; Huang, Z.; Ding, B.; and Li, Y. 2020. Simple and Deep Graph Convolutional Networks. In *ICML*, 1725–1735.
- Cheng, J.; Wang, Q.; Tao, Z.; and Gao, Q. 2020. Multi-View Attribute Graph Convolution Networks for Clustering. In *IJCAI*, 2973–2979.
- Chenghua, L.; Zhuolin, L.; Yixuan, M.; and Kun, Z. 2022. Stationary Diffusion State Neural Estimation for Multiview Clustering. In *AAAI*, 7542–7549.
- Dilokthanakul, N.; Mediano, P. A.; Garnelo, M.; Lee, M. C.; Salimbeni, H.; Arulkumaran, K.; and Shanahan, M. 2016. Deep unsupervised clustering with gaussian mixture variational autoencoders. *arXiv preprint arXiv:1611.02648*.
- Elinas, P.; Bonilla, E. V.; and Tiao, L. C. 2020. Variational Inference for Graph Convolutional Networks in the Absence of Graph Data and Adversarial Settings. In *NeuIPS*.
- Fan, S.; Wang, X.; Shi, C.; Lu, E.; Lin, K.; and Wang, B. 2020. One2Multi Graph Autoencoder for Multi-view Graph Clustering. In *WWW*, 3070–3076.
- Gilbert, E. N. 1959. Random Graphs. Ann Stat, 30(4): 1141 1144.
- Hassani, K.; and Khasahmadi, A. H. 2020. Contrastive multi-view representation learning on graphs. In *ICML*, 4116–4126.
- Jang, E.; Gu, S.; and Poole, B. 2016. Categorical reparameterization with gumbel-softmax. *arXiv* preprint arXiv:1611.01144.
- Kingma, D. P.; and Welling, M. 2014. Auto-Encoding Variational Bayes. In *ICLR*.
- Kipf, T. N.; and Welling, M. 2016. Variational graph autoencoders. In *NeuIPS*.
- Kipf, T. N.; and Welling, M. 2017. Semi-Supervised Classification with Graph Convolutional Networks. In *ICLR*.
- Lin, Y.; Gou, Y.; Liu, Z.; Li, B.; Lv, J.; and Peng, X. 2021. COM-PLETER: Incomplete multi-view clustering via contrastive prediction. In *CVPR*, 11174–11183.
- Lin, Z.; and Kang, Z. 2021. Graph filter-based multi-view attributed graph clustering. In *IJCAI*, 19–26.
- Liu, W.; Chen, P.-y.; Yeung, S.; Suzumura, T.; and Chen, L. 2017. Principled multilayer network embedding. In *ICDMW*, 134–141.
- Luo, D.; Cheng, W.; Xu, D.; Yu, W.; Zong, B.; Chen, H.; and Zhang, X. 2020. Parameterized Explainer for Graph Neural Network. In *NeuIPS*.
- Maaten, L. v. d.; and Hinton, G. 2008. Visualizing Data using t-SNE. *JMLR*, 9(2605): 2579–2605.
- Macqueen, J. 1967. Some methods for classification and analysis of multivariate observations. In *In 5-th Berkeley Symposium on Mathematical Statistics and Probability*, 281–297.
- Maddison, C. J.; Mnih, A.; and Teh, Y. W. 2016. The concrete distribution: A continuous relaxation of discrete random variables. *arXiv preprint arXiv:1611.00712*.
- Morris, C.; and Mutzel, P. 2020. Towards a practical k-dimensional Weisfeiler-Leman algorithm. In *NeurIPS*.

- Nie, F.; Li, J.; and Li, X. 2017. Self-weighted Multiview Clustering with Multiple Graphs. In *IJCAI*, 2564–2570.
- Nie, F.; Li, J.; Li, X.; et al. 2017. Self-weighted Multiview Clustering with Multiple Graphs. In *IJCAI*, 2564–2570.
- Pan, E.; and Kang, Z. 2021. Multi-view Contrastive Graph Clustering. *NeurIPS*, 34: 2148–2159.
- Pan, S.; Hu, R.; Long, G.; Jiang, J.; Yao, L.; and Zhang, C. 2018. Adversarially Regularized Graph Autoencoder for Graph Embedding. In *IJCAI*, 2609–2615.
- Sun, L.; Zhang, Z.; Zhang, J.; Wang, F.; Peng, H.; Su, S.; and Yu, P. S. 2021. Hyperbolic Variational Graph Neural Network for Modeling Dynamic Graphs. In *AAAI*.
- Tang, C.; Liu, X.; Zhu, X.; Zhu, E.; Luo, Z.; Wang, L.; and Gao, W. 2020. CGD: Multi-View Clustering via Cross-View Graph Diffusion. In *AAAI*.
- Tang, J.; Qu, M.; Wang, M.; Zhang, M.; Yan, J.; and Mei, Q. 2015. Line: Large-scale information network embedding. In *WWW*, 1067–1077.
- Tishby, N.; Pereira, F. C.; and Bialek, W. 2000. The information bottleneck method. *arXiv preprint physics/0004057*.
- Vaswani, A.; Shazeer, N.; Parmar, N.; Uszkoreit, J.; Jones, L.; Gomez, A. N.; Kaiser, L.; and Polosukhin, I. 2017. Attention is All You Need. In *NeuIPS*, 6000–6010.
- Velickovic, P.; Fedus, W.; Hamilton, W. L.; Liò, P.; Bengio, Y.; and Hjelm, R. D. 2019. Deep Graph Infomax. *ICLR*.
- Veličković, P.; Cucurull, G.; Casanova, A.; Romero, A.; Liò, P.; and Bengio, Y. 2018. Graph Attention Networks. In *ICLR*.
- Wang, C.; Pan, S.; Hu, R.; Long, G.; Jiang, J.; and Zhang, C. 2019. Attributed Graph Clustering: A Deep Attentional Embedding Approach. In *IJCAI*, 3670–3676. AAAI Press.
- Wang, C.; Pan, S.; Yu, C. P.; Hu, R.; Long, G.; and Zhang, C. 2022. Deep neighbor-aware embedding for node clustering in attributed graphs. *Pattern Recognit.*, 122: 108230.
- Wang, H.; Yang, Y.; and Liu, B. 2020. GMC: Graph-Based Multi-View Clustering. *TKDE*, 32(6): 1116–1129.
- Wu, F.; Jr., A. H. S.; Zhang, T.; Fifty, C.; Yu, T.; and Weinberger, K. Q. 2019. Simplifying Graph Convolutional Networks. In *ICML*, 6861–6871.
- Xia, R.; Pan, Y.; Du, L.; and Yin, J. 2014. Robust Multi-View Spectral Clustering via Low-Rank and Sparse Decomposition. In *AAAI*, 2149–2155.
- Xie, J.; Girshick, R.; and Farhadi, A. 2016. Unsupervised Deep Embedding for Clustering Analysis. In *ICML*, 478–487.
- Xu, J.; Ren, Y.; Li, G.; Pan, L.; Zhu, C.; and Xu, Z. 2021a. Deep embedded multi-view clustering with collaborative training. *Inf. Sci.*, 573: 279–290.
- Xu, J.; Ren, Y.; Tang, H.; Pu, X.; Zhu, X.; Zeng, M.; and He, L. 2021b. Multi-VAE: Learning Disentangled View-common and View-peculiar Visual Representations for Multi-view Clustering. In *ICCV*, 9214–9223.
- Xu, K.; Hu, W.; Leskovec, J.; and Jegelka, S. 2019. How Powerful are Graph Neural Networks? In *ICLR*.
- Zhan, K.; Nie, F.; Wang, J.; and Yang, Y. 2018. Multiview consensus graph clustering. *TIP*, 28(3): 1261–1270.
- Zhang, X.; Liu, H.; Li, Q.; and Wu, X.-M. 2019. Attributed Graph Clustering via Adaptive Graph Convolution. In *IJCAI*, 4327–4333.
- Zheng, C.; Zong, B.; Cheng, W.; Song, D.; Ni, J.; Yu, W.; Chen, H.; and Wang, W. 2020. Robust Graph Representation Learning via Neural Sparsification. In *ICML*, 11458–11468.
- Zhu, H.; and Koniusz, P. 2021. Simple Spectral Graph Convolution. In  $\mathit{ICLR}$ .

### **A** Overall Notations

The explanations of all notations are shown in Table 8 on the final page.

### **B** More Related Works

# **B.1** Graph Neural Networks for Multi-View Graph Clustering

Xu et al. (2019) has theoretically proved that GNNs can efficiently embed graph structural information with features. Promoted by the success of GNNs, several multi-view clustering methods have emerged. Specifically, Fan et al. (2020) first employed GNN (Kipf and Welling 2017) for MGC. It selects an informative graph with features and conducts GNN to generate embeddings for clustering, and multi-view information is injected by backpropagation. However, the information implied in unselected graphs are largely lost by this way. Cheng et al. (2020) adopted GNN on multiple features with a shared graph, but it cannot be generalized to the data with multiple graphs. Alternatively, researchers in (Pan and Kang 2021) and (Lin and Kang 2021) embedded each graph's information in each view separately via graph filter, and then learned a consensus graph which will be partitioned to different clusters. However, due to their clustering results only being determined by the generated graph, some useful information in features is ignored. Recently, Chenghua et al. (2022) proposed stationary diffusion state neural estimation (SDSNE) for multi-view clustering, which utilizes the stationary diffusion to get a consensus graph, and performs the spectral clustering on this graph directly. However, in essence, SDSNE belongs to the first type, so it also suffers from the inherent issues of this type, i.e., the clustering results determined by the consensus graph, and some feature information is lost. Differently, the proposed VGMGC could reserve useful feature information, and utilize the powerful graph embedding ability of GNNs to assimilate both the consensus and specific graph information for clustering task.

# C Details of Datasets and Comparison Methods

### C.1 Details of Datasets

Four common benchmark graph datasets, *i.e.*, ACM, DBLP, Amazon photos and Amazon computers, are selected to evaluate the proposed SAMGC. ACM and DBLP are multigraph datasets, while Amazon photos and Amazon computers only consist of single-view features. Specifically,

- ACM<sup>1</sup>: This is a paper network from the ACM database. It consists of two different graphs, co-paper and co subject, represents the relationship of the same author with papers and the relationship of the same subject with papers respectively. The node feature is a bag-of-words representation of each paper's keywords.
- DBLP<sup>2</sup>: This is an author network from the DBLP database. The dataset includes three graphs, *i.e.* coauthor (co-authors for the same paper), co-conference

- (papers published on the same conference) and co-term (papers published on the same term). The node feature is a bag-of-words representation of each author's keywords.
- Amazon datasets: Amazon photos and Amazon computers are the subsets of the Amazon co-purchase network from (Pan and Kang 2021). The network means the two goods that are purchased together. The node feature is a bag-of-words representation of each good's product reviews. Due to Amazon photos and Amazon computers only having single-view features, we constructed the second view features through cartesian product following by (Cheng et al. 2020).
- Cora<sup>3</sup> and Citeseer<sup>4</sup>: Cora and Citeseer are two classical single-view graph datasets. Each node represent a paper with features extracted from bag-of-word of the paper. The network is a paper citation network.
- BBC Sport<sup>5</sup>: BBC Sport is a widely-used traditional multi-view dataset. Each node is a document from one of five classes with two features extracted from the document. Two graphs are constructed from features in SD-SNE (Chenghua et al. 2022).
- Three Sources<sup>6</sup>: Three Sources is a traditional multiview dataset, containing 169 reports reported in different three sources. Each node represents a reports with three features extracted from three sources respectively. The graphs are constructed from features in SD-SNE (Chenghua et al. 2022).

The statistics information of these datasets are listed in Table 4.

### **C.2** Details of Comparison Methods

Our comparison methods in Table 1 can be divided into three categories:

- LINE & GAE: LINE (Tang et al. 2015) and GAE (Kipf and Welling 2016) are two typical single-view clustering methods.
- Baselines: RMSC (Xia et al. 2014), PMNE (Liu et al. 2017), SwMC (Nie et al. 2017) and MNE (Zhan et al. 2018) are four classical multi-view clustering methods. All of them are graph embedding models, except RMSC is a robust spectral clustering model.
- SOTAs: O2MAC (Fan et al. 2020) and MAGCN (Cheng et al. 2020) are the methods that learn from both attribute features and structural information. In addition, graph filter-based MGC methods, like MvAGC (Lin and Kang 2021) and MCGC (Pan and Kang 2021), are included. COMPLETER (Lin et al. 2021) and MVGRL (Hassani and Khasahmadi 2020) are contrastive learning methods to learn a common representation for clustering.

Our comparison methods in Appendix E Table 7 can be divided into two streams:

<sup>1</sup>https://dl.acm.org/

<sup>&</sup>lt;sup>2</sup>https://dblp.uni-trier.de/

<sup>&</sup>lt;sup>3</sup>https://linqs-data.soe.ucsc.edu/public/lbc/cora.tgz

<sup>4</sup>http://www.cs.umd.edu/ sen/lbc-proj/data/citeseer.tgz

<sup>&</sup>lt;sup>5</sup>http://mlg.ucd.ie/datasets/bbc.html

<sup>&</sup>lt;sup>6</sup>http://mlg.ucd.ie/datasets/3sources.html

Dataset	#Clusters	#Nodes	#Features	Graphs
ACM	3	3025	1830	$\mathcal{G}^1$ co-paper $\mathcal{G}^2$ co-subject
DBLP	4	4057	334	$\mathcal{G}^1$ co-author $\mathcal{G}^2$ co-conference $\mathcal{G}^3$ co-term
Amazon photos	8	7487	745 7487	$\mathcal{G}^1$ co-purchase
Amazon computers	10	13381	767 13381	$\mathcal{G}^1$ co-purchase
Cora	7	2708	1433	$\mathcal{G}^1$ paper citation network
Citeseer	6	3327	3703	$\mathcal{G}^1$ paper citation network
BBC Sport	5	544	3283 3183	$\mathcal{G}^1$ constructed from features $\mathcal{G}^2$ constructed from features
Three Sources	6	169	3560 3631 3068	$\mathcal{G}^1$ constructed from features $\mathcal{G}^2$ constructed from features $\mathcal{G}^3$ constructed from features

Table 4: The statistics information of the four multi-graph datasets.

- Single-view graph clustering methods: VGAE (Kipf and Welling 2016), ARVGE (Pan et al. 2018), and GMM-VGAE (Binyuan, Pengfei, and Qinghua 2020) are three variational-based methods; DNENC (Wang et al. 2022) and MAGCN (Cheng et al. 2020) are two SOTAs conducted on single-view graph data.
- Traditional multi-view clustering methods: GMC (Wang, Yang, and Liu 2020), CGD (Tang et al. 2020) and SD-SNE (Chenghua et al. 2022) are three graph-based multiview clustering SOTAs. They learn a unified graph from multi-view data for multi-view clustering; O2MAC (Fan et al. 2020) conducts GNN for multi-view clustering.

### **C.3** Details of Metrics

Following the work of the pioneers, we adopt four common metrics, *i.e.* normalized mutual information (NMI), adjusted rand index (ARI), accuracy (ACC) and F1-score (F1), as the metrics to evaluate the clustering performance of the proposed VGMGC. For comparison, we collect the best reported performance from the literature.

### **D** Proofs and Derivations

### **D.1** Detailed Derivation of Formulas

**Derivation of the Mutual Information (Eq. (5))** Recall Eq. (4):

$$\alpha = \mathbf{K}\mathbf{Q}^T$$
, where  $\mathbf{K} = f'(\overline{\mathbf{X}}), \mathbf{Q} = \mathbf{K}\mathbf{W}$ , (24)

which implies that the information in  $\alpha$  is determinstic given K and Q. So, we have:

$$\max I(\alpha, \overline{\mathbf{X}}) \Rightarrow \max I(\mathbf{K}, \overline{\mathbf{X}}) \text{ and } \max I(\mathbf{Q}, \overline{\mathbf{X}}).$$

Considering the three variables K, Q and  $\overline{X}$ , we have Markov chain:  $\overline{X} \to K \to Q$ . According to Data Processing Inequality:

$$I(\mathbf{K}, \overline{\mathbf{X}}) \ge I(\mathbf{Q}, \overline{\mathbf{X}}),$$

which demonstrates that  $I(\mathbf{Q}, \overline{\mathbf{X}})$  is the lower bound of  $I(\mathbf{K}, \overline{\mathbf{X}})$ . So we obtain Eq. (5):

$$\max I(\boldsymbol{\alpha}, \overline{\mathbf{X}}) \Rightarrow \max I(\mathbf{K}, \overline{\mathbf{X}}) \text{ and } \max I(\mathbf{Q}, \overline{\mathbf{X}}) \cong \max I(\mathbf{Q}, \overline{\mathbf{X}}). \tag{25}$$

**Derivation of Evidence Lower Bound (Eq.** (8)) We can derive Eq. (8)) via Jensen's inequality and our Bayesian net (Figure 4):

$$\begin{split} &\sum_{v=1}^{V} \log p(\mathbf{A}^{v}) = \sum_{v=1}^{V} \log \int \int p(a^{v}, \hat{s}, x^{v}) d\hat{s} dx^{v} \\ &= \sum_{v=1}^{V} \log \int \int \frac{q(\hat{s} \mid \overline{x})}{q(\hat{s} \mid \overline{x})} p(a^{v}, \hat{s}, x^{v}) d\hat{s} dx^{v} \\ &= \sum_{v=1}^{V} \log \int \mathbb{E}_{q(\hat{s} \mid \overline{x})} \frac{p(a^{v}, \hat{s}, x^{v})}{q(\hat{s} \mid \overline{x})} dx^{v} \\ &\geq \sum_{v=1}^{V} \mathbb{E}_{q(\hat{s} \mid \overline{x})} \log \int \frac{p(a^{v}, \hat{s}, x^{v})}{q(\hat{s} \mid \overline{x})} dx^{v}, \text{ (Jensen's inequality),} \\ &= \sum_{v=1}^{V} \mathbb{E}_{q(\hat{s} \mid \overline{x})} \log \int \frac{p(a^{v} \mid \hat{s}, x^{v}) p(\hat{s})}{q(\hat{s} \mid \overline{x})} p(x^{v}) dx^{v}, \text{ ($\hat{s} \perp x^{v} \mid \emptyset),} \\ &= \sum_{v=1}^{V} \mathbb{E}_{q(\hat{s} \mid \overline{x})} \log p(a^{v} \mid \hat{s}, x^{v}) - \mathbb{E}_{q(\hat{s} \mid \overline{x})} \log \frac{p(\hat{s})}{q(\hat{s} \mid \overline{x})} \\ &= \sum_{v=1}^{V} \mathbb{E}_{q(\hat{s} \mid \overline{x})} \log p(a^{v} \mid \hat{s}, x^{v}) - KL(q(\hat{s} \mid \overline{x}) || p(\hat{s})). \end{split}$$

Here,  $\hat{s} \perp x^v \mid \emptyset$  is derived from the Bayesian net (Figure 4).

**Derivation of the Message-Passing Method (Eq.** (10)) Let  $\mathbf{E}^{(l)}$  be the embedding of l-th layer, the definition of

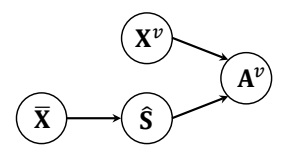


Figure 4: The Bayesian net of variables:  $\mathbf{A}^v$ ,  $\hat{\mathbf{S}}$ ,  $\overline{\mathbf{X}}$  and  $\mathbf{X}^v$ .

vanilla Graph Convolutional Neural Networks (GCN) (Kipf and Welling 2017) is as followes:

**Definition 3.** The vanilla GCN is defined as:

$$\mathbf{E}^{(l+1)} = (\widetilde{\mathbf{A}}\mathbf{E}^{(l)}\mathbf{W}^{(l)}), \text{ where } \mathbf{E}^{(0)} = \mathbf{X}. \tag{27}$$

We first remove the unnecessary parameters **W** from Eq. (27), and then, add a residual connection to every layer from the input features **X**. Therefore, the improved parameter-free graph neural network could be written as:

$$\mathbf{E}^{(l+1)} = \widetilde{\mathbf{A}} \mathbf{E}^{(l)} + \mathbf{X}. \tag{28}$$

Finally, it is easy to prove the following formula via mathematical induction:

$$\mathbf{E}^{(order)} = \left(\sum_{l=0}^{order} \widetilde{\mathbf{A}}^l + \mathbf{I}\right) \mathbf{X}.$$
 (29)

### D.2 Proofs in Section 3.6

**Proof of Proposition 1.** Assume all graphs are equally reliable, the more consistent the observed graphs are, the less uncertain the consensus graph is, and vice versa:

$$H(\hat{\mathbf{S}}) \propto d_{Ham}(\mathbf{A}^1, \mathbf{A}^2).$$
 (30)

**Proof.** Assume there are two views with equal belief, i.e., V=2 and  $b^1=b^2=b$ , we have:

$$\log \beta_{ij} = \log \frac{b(a_{ij}^1 + a_{ij}^2) + (1 - b)(a_{ij}^1 + a_{ij}^2)}{2b}.$$
 (31)

Note that KL divergence is always positive, so, from Eq. (9), we have :

$$KL\left(q_{\phi'}(\hat{\mathbf{S}} \mid \overline{\mathbf{X}}) \parallel p(\hat{\mathbf{S}})\right) = -H(\hat{\mathbf{S}}) + \sum_{ij} \log \frac{1}{\beta_{ij}} \ge 0$$

$$\Rightarrow H(\hat{\mathbf{S}}) \le \sum_{ij} \log \frac{1}{\beta_{ij}}$$

$$= \sum_{ij} \log \frac{2b}{b(a_{ij}^{1} + a_{ij}^{2}) + (1 - b)(2 - (a_{ij}^{1} + a_{ij}^{2}))}$$

$$= \sum_{ij} \log 2b - \sum_{ij} C_{ij},$$
(32)

where  $C_{ij} = \log b(a_{ij}^1 + a_{ij}^2) + (1 - b)(2 - (a_{ij}^1 + a_{ij}^2)),$  and we have:

$$C_{ij} = \begin{cases} \log(b+1-b) = 0, & \text{if } a_{ij}^1 \neq a_{ij}^2, \\ \log 2b, & \text{if } a_{ij}^1 = a_{ij}^2 = 1, \\ \log 2(1-b), & \text{if } a_{ij}^1 = a_{ij}^2 = 0. \end{cases}$$
(33)

Let n, t and k be the number of all edges,  $a_{ij}^1 = a_{ij}^2 = 1$  and  $a_{ij}^1 = a_{ij}^2 = 0$  respectively, so we have:

$$H(\mathbf{\hat{S}}) \le n\log 2b - t\log 2b - k\log 2(1-b). \tag{34}$$

Considering  $d_{Ham} = \sum_{ij} |a_{ij}^1 - a_{ij}^2| = n - t - k$ , we have:

$$H(\hat{\mathbf{S}}) \le d_{Ham} \log 2b + k \log \frac{b}{1-b}.$$
 (35)

So, the maximized  $H(\hat{\mathbf{S}})$  is proportional to  $d_{Ham}$ , i.e.,  $H(\hat{\mathbf{S}}) \propto d_{Ham}$ .

**Proof of Proposition 2.** For a specific graph, the more this graph relative to the clustering task, the more the distribution of  $\hat{S}$  similar to it, and vice versa:

$$H(\mathbf{A}^v, \hat{\mathbf{S}}) \propto b^v.$$
 (36)

Proof.

$$H(\mathbf{A}^{v}, \hat{\mathbf{S}})$$

$$= \sum_{ij} p(a_{ij}^{v}) \log \frac{1}{p(\hat{s}_{ij})}$$

$$= \sum_{ij} [b^{v} a_{ij}^{v} + (1 - b^{v})(1 - a_{ij}^{v})] \log \frac{1}{\beta_{ij}}$$

$$= b^{v} \sum_{ij} (2a_{ij}^{v} - 1) \log \frac{1}{\beta_{ij}} + \sum_{ij} \log \frac{1}{\beta_{ij}} - \sum_{ij} a_{ij}^{v} \log \frac{1}{\beta_{ij}}$$

$$\Rightarrow H(\mathbf{A}^{v}, \hat{\mathbf{S}}) \propto b^{v}.$$
(37)

**Proof of Theorem 1.** The distribution of  $\hat{\mathbf{S}}$  is dependent on the consistency of observed graphs and how much they are related to the clustering task.

**Proof.** Recall our assumption:  $p(\hat{\mathbf{S}}) = \prod_{i,j} p(\hat{s}_{ij}) = \prod_{i,j} p(\hat{s}_{ij} = 1) = \prod_{i,j} \beta_{ij}$ , we have:

$$p(\hat{\mathbf{S}}) \propto \boldsymbol{\beta}.$$
 (38)

From Eq. (3), we can easily obtain that  $p(\hat{\mathbf{S}}) \propto \beta \propto \{b^v\}, \{\mathbf{A}^v\}$ . Here,  $b^v$  determines how much the v-the view is related to the clustering task,  $\{\mathbf{A}^v\}$  determines the consistency of observed graphs. So we obtain this theorem.

Furthermore, we also can conclude this theorem from Proposition 1. and Proposition 2. directly.

**Proof of Theorem 2.** Maximizing the ELBO Eq. (8) is equivalent to maximizing IB when  $\omega = 1$ :

$$\max \mathcal{L}_E \cong \max \mathcal{IB}_{var}. \tag{39}$$

Here,  $\mathcal{IB}_{var}$  is defined in Definition 2:

**Definition 2.** The IB in our variational graph generator is:

$$\mathcal{IB}_{var} = \sum_{v} I(\mathbf{A}^{v}, \hat{\mathbf{S}}) - \omega I(\hat{\mathbf{S}}, \overline{\mathbf{X}}), \text{ where } \omega > 0.$$
 (40)

**Proof.** For simplification, we rewrite mutual information as  $I(\cdot;\cdot)$ ;  $\mathbf{A}$ ,  $\overline{\mathbf{X}}$ ,  $\mathbf{X}^v$  and  $\hat{\mathbf{S}}$  as A,  $\overline{X}$ ,  $X^v$  and  $\hat{S}$ . Recall the property of mutual information:

$$I(X;Y \mid Z) = I(X;Y) + H(Z \mid X) + H(Z \mid Y) - H(Z \mid X,Y) - H(Z),$$
(41)

where,  $H(\cdot)$  denotes Entropy. From this property, we have:

$$I(A^{v}; \hat{S} \mid \overline{X}, X^{v}) = I(A^{v}; \hat{S}) + H(\overline{X}, X^{v} \mid \hat{S}) + H(\overline{X}, X^{v} \mid A^{v}) - H(\overline{X}, X^{v} \mid A, \hat{S}) - H(\overline{X}, X^{v}).$$
(42)

Note that  $\overline{X}$  and  $X^v$  are observed, so  $H(\overline{X})$  and  $H(X^v)$  are two constants. We have:

$$I(A; \hat{S}) \propto I(A^v; \hat{S} \mid \overline{X}, X^v).$$

The Bayesian network for the variables  $A^v$ ,  $\hat{S}$ ,  $\overline{X}$  and  $X^v$  is depicted in Figure 4.

From Figure 4, we have the following derivation:

$$\begin{split} &I(A^{v}; \hat{S} \mid \overline{X}, X^{v}) \\ &= \mathbb{E}_{p(\overline{x}, x^{v})} \int \int p(a^{v}, \hat{s} \mid \overline{x}, x^{v}) \log \frac{p(a^{v}, \hat{s} \mid \overline{x}, x^{v})}{p(a^{v} \mid \overline{x}, x^{v})} p(\hat{s} \mid \overline{x}, x^{v}) d\hat{s} da^{v} \\ &= \mathbb{E}_{p(\overline{x})p(x^{v})} \int \int p(a^{v} \mid x^{v}) p(\hat{s} \mid \overline{x}) \log \frac{p(a^{v} \mid \hat{s}, x^{v})}{p(a^{v} \mid x^{v})} d\hat{s} da^{v} \\ &= \mathbb{E}_{p(\overline{x})p(x^{v})} \int \int p(a^{v} \mid x^{v}) p(\hat{s} \mid \overline{x}) \log p(a^{v} \mid \hat{s}, x^{v}) d\hat{s} da^{v} + H(A^{v}) \\ &\geq \mathbb{E}_{p(\overline{x})p(x^{v})} \int \int p(a^{v} \mid x^{v}) p(\hat{s} \mid \overline{x}) \log p(a^{v} \mid \hat{s}, x^{v}) d\hat{s} da^{v} \\ &\geq \mathbb{E}_{p(\overline{x})p(x^{v})} \mathbb{E}_{p(a^{v} \mid x^{v})p(\hat{s} \mid \overline{x})} \log q(a^{v} \mid \hat{s}, x^{v}), \end{split}$$

where  $q(a^v \mid \hat{s}, x^v)$  is a variational approximation of  $p(a^v \mid \hat{s}, x^v)$ . The last term of Eq. (43) is deduced from  $KL(p(a^v \mid \hat{s}, x^v)) | q(a^v \mid \hat{s}, x^v)) \geq 0$ . Therefore, we have obtained the first term in  $\mathcal{L}_E$  from Eq. (43). For the second term, we have:

$$I(\hat{S}, \overline{X}) = \int \int \log \frac{p(\hat{s}, \overline{x})}{p(\hat{s})p(\overline{x})} d\overline{x} d\hat{s}$$

$$= \mathbb{E}_{p(\overline{x})} \int p(\hat{s} \mid \overline{x}) \log p(\hat{s} \mid \overline{x}) d\hat{s}$$

$$= \mathbb{E}_{p(\overline{x})} KL \left( p(\hat{s} \mid \overline{x}) \| p(\hat{s}) \right). \tag{44}$$

Therefore, we have obtained the second term in  $\mathcal{L}_E$  from Eq. (44). Theorem 2. can be obtained by concluding the above formulas:

$$\max I(A^{v}, \hat{S}) - I(\hat{S}, \overline{X}) \cong \max \mathbb{E}_{p(a^{v} \mid x^{v})p(\hat{s} \mid \overline{x})} \log q(a^{v} \mid \hat{s}, x^{v}) \\ - KL(p(\hat{s} \mid \overline{x}) \| p(\hat{s}))$$

$$\Rightarrow \max \mathcal{IB}_{var} \cong \max \mathcal{L}_{E}.$$

$$(45)$$

**Proof of Theorem 3.** Maximizing mutual information is equivalent to maximizing its lower bound:

$$\max I(\mathbf{Z}^{v}, \mathbf{X}^{v}) \cong \max \mathbb{E}_{q_{\eta^{v}}(\mathbf{x}^{v} \mid \mathbf{z}^{v})} \log q_{\eta^{v}}(\mathbf{x}^{v} \mid \mathbf{z}^{v}). \tag{46}$$

**Proof.** Considering that the entropy  $H(\cdot)$  is always positive,

we have:

$$I(\mathbf{Z}^{v}, \mathbf{X}^{v})$$

$$= \int \int p(\mathbf{z}^{v}, \mathbf{x}^{v}) \log \frac{p(\mathbf{x}^{v} \mid \mathbf{z}^{v})}{p(\mathbf{x}^{v})} d\mathbf{x}^{v} d\mathbf{z}^{v}$$

$$= \int \int p(\mathbf{x}^{v}) p(\mathbf{z}^{v} \mid \mathbf{x}^{v}) \log p(\mathbf{x}^{v} \mid \mathbf{z}^{v}) d\mathbf{x}^{v} d\mathbf{z}^{v}$$

$$+ \int \int p(\mathbf{x}^{v}) p(\mathbf{z}^{v} \mid \mathbf{x}^{v}) \log \frac{1}{p(\mathbf{x}^{v})} d\mathbf{x}^{v} d\mathbf{z}^{v}$$

$$= \int \int p(\mathbf{x}^{v}) p(\mathbf{z}^{v} \mid \mathbf{x}^{v}) \log p(\mathbf{x}^{v} \mid \mathbf{z}^{v}) d\mathbf{x}^{v} d\mathbf{z}^{v} + H(\mathbf{X}^{v})$$

$$\geq \int \int p(\mathbf{x}^{v}) p(\mathbf{z}^{v} \mid \mathbf{x}^{v}) \log p(\mathbf{x}^{v} \mid \mathbf{z}^{v}) d\mathbf{x}^{v} d\mathbf{z}^{v}.$$

Let  $q(\mathbf{x}^v \mid \mathbf{z}^v)$  be a variational approximation of  $p(\mathbf{x}^v \mid \mathbf{z}^v)$ . Considering that KL divergence is always positive, i.e.,  $KL(p(\mathbf{x}^v \mid \mathbf{z}^v) || q(\mathbf{x}^v \mid \mathbf{z}^v)) \geq 0$ , we can obtain that:

$$\int \int p(\mathbf{x}^{v})p(\mathbf{z}^{v} \mid \mathbf{x}^{v}) \log p(\mathbf{x}^{v} \mid \mathbf{z}^{v}) d\mathbf{x}^{v} d\mathbf{z}^{v} 
\geq \int \int p(\mathbf{x}^{v})p(\mathbf{z}^{v} \mid \mathbf{x}^{v}) \log q(\mathbf{x}^{v} \mid \mathbf{z}^{v}) d\mathbf{x}^{v} d\mathbf{z}^{v}.$$
(48)

Finally, we obtain the lower bound of mutual information:

$$I(\mathbf{Z}^{v}, \mathbf{X}^{v}) \geq \int \int p(\mathbf{x}^{v}) p(\mathbf{z}^{v} \mid \mathbf{x}^{v}) \log q(\mathbf{x}^{v} \mid \mathbf{z}^{v}) d\mathbf{x}^{v} d\mathbf{z}^{v}$$

$$= \mathbb{E}_{p(\mathbf{x}^{v}) p(\mathbf{z}^{v} \mid \mathbf{x}^{v})} \log q(\mathbf{x}^{v} \mid \mathbf{z}^{v}) d\mathbf{x}^{v}.$$
(49)

### **E** More Experiments

### **E.1** More Results of Sensitive Analysis

Here presents more results about sensitive analysis of accuracy with  $\rho$  and  $\tau$ . From Figure 5, we can conclude that VGMGC is not sensitive to hyper-parameter  $\rho$  and  $\tau$ , with the variation of accuracy is within 3%.

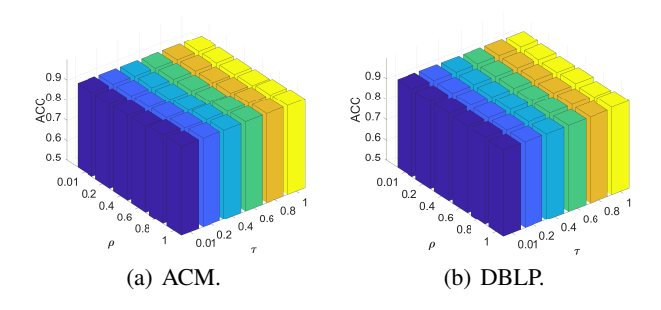


Figure 5: Sensitive analysis of accuracy with  $\rho$  and  $\tau$ .

Furthermore, we explore a wider range of  $\tau$  to see how it influences the distribution of generated graph. The distribution of generated graph is represented by the mean and variance of  $s_{ij}$ . From Table 5, the variance of  $s_{ij}$  falls and its mean value closes to 50% gradually as  $\tau$  increasing. This is because increasing  $\tau$  injects more noise whose distribution subjects to Uniform(0,1) to  $s_{ij}$ , which is consistent with the theory.

Temperature	NMI%	ARI%	ACC%	F1%	Mean of $s_{ij}$ (1e-2)	Variance of $s_{ij}$ (1e-2)
$\tau = 0.1$	77.4	82.6	93.8	93.9	50.46	22.5
$\tau = 1$	77.5	82.8	93.9	93.9	50.297	8.337
$\tau = 2$	77.7	82.9	94.0	94.0	50.192	3.542
au=5	77.7	83.1	94.1	94.1	50.091	0.758
$\tau = 10$	77.7	83.0	94.0	94.0	50.046	0.201
$\tau = 50$	77.6	83.0	94.0	94.0	50.009	8.217 (1e-5)
$\tau = 100$	77.2	82.7	93.9	93.9	50.0004	2.056 (1e-5)

Table 5: Experiments of larger  $\tau$  on ACM. The mean and variance of  $s_{ij}$  are computed from the 200th epoch.

### E.2 More Results of Ablation Study

Table 6 shows the results of ablation study conducted on the Amazon photos dataset. As discussed in Section 4.3, the consensus graph  $\hat{\mathbf{S}}$  and reconstruction constraint  $\mathcal{L}_r$  make significant contributions to the performance of the whole VGMGC model. Notably, although single  $\mathcal{G}^1$  and  $\mathcal{G}^2$  have ordinary performance, VGMGC can make good use of the complementary information between views when multiple views are fed into the model.

### E.3 Experiments on More Datasets

As shown in Table 7, we experiment on two single-view graph datasets, *i.e.*, Cora and Citeseer, and two traditional multi-view datasets, *i.e.*, BBC Sport and Three Sources. The results show that VGMGC performs best compared to several SOTAs, demonstrating that the proposed method can be well adapted to both single-view graph clustering and traditional multi-view clustering tasks.

### E.4 Visualization of Each View

In order to obtain a more intuitive understanding of the clustering performance of the proposed VGMGC, each view obtained finally is visualized in Figure 6. Each view has either good or bad clustering results, for example,  $\mathbf{Z}^3$  in DBLP perform poorly, while  $\mathbf{Z}^2$  in DBLP perform relatively well. Nevertheless, the generated variational consensus graph  $\overline{\mathbf{Z}}$  still manages to have an impressive performance because it can mine enough view-specific and view-common information from the different views. This corroborates the results in Section 4.4).

### F Implementation Details

The experiments are conducted on a CentOS machine with a NVIDIA Tesla V100 SXM2 GPU and Cascade LakeP82 v6@2.4GHz CPU. CUDA version is 10.2 and PyTorch version is 1.11.0. The implementation of VGMGC will be public available.

### **F.1** Details of Inference Process

The variational consensus graph  $\hat{\mathbf{S}}$  is generated through a f' from global features  $\overline{\mathbf{X}}$ . The instantiation of f' is an MLP, playing a role of encoder to extract the information from  $\overline{\mathbf{X}}$ . Specifically, f' consists of three layers, *i.e.*,  $input \rightarrow hidden \rightarrow output$ , and each layer follows a Dropout operation. In our model, we set the dimensions of both hidden

and output layers as 512, drop rate of Dropout operation as 0.1 and all parameters of  $\phi'$  are initialized with Xavier.

## F.2 Details of Global and Specific Graph Encoder

Similar to the MLP f',  $f_v$  also has three layers, the dimensions of hidden and output layers are chosen to be 512. The parameters  $\phi^v$  are initialized with Kaiming, and ReLu is selected as the activation function.

### F.3 Details of Loss Functions

Reconstruction Loss in Evidence Lower Bound Loss In the generative process, the decoder of  $p_{\xi}^v(\mathbf{A}^v|\hat{\mathbf{S}},\mathbf{X}^v)$  shares structure and parameters with  $f_v$  and  $\phi^v$ . Finally,  $\check{\mathbf{A}}^v$  can be reconstructed through  $\sigma(\mathbf{Z}^v(\mathbf{Z}^v)^\top)$ , where  $\sigma(\cdot)$  denotes Sigmoid function. Thus  $\mathcal{L}_E$  can be written as:

$$\mathcal{L}_E = -\sum_{v=1}^{V} H(\mathbf{A}^v, \check{\mathbf{A}}^v) + H(\hat{\mathbf{S}}) - \sum_{ij} \log \frac{1}{\beta_{ij}}.$$
 (50)

**Lower Bound of Mutual Information Loss** For the reconstruction of  $\mathbf{X}^v$ ,  $\mathbf{Z}^v$  is fed into an MLP decoder, whose structure is the opposite of  $f_v$ . To reconstruct the global features  $\overline{\mathbf{X}}$  to  $\overline{\mathbf{X}}$ , the obtained  $\mathbf{Q}$  is fed into an MLP decoder opposite of f'. Subsequently, the reconstruction losses  $\mathcal{L}_v^v$  and  $\mathcal{L}_r'$  for maximizing the lower bound of mutual information can be written as follows:

$$\mathcal{L}_r^v = \sum_{v=1}^V H(\mathbf{X}^v, \check{\mathbf{X}}^v)$$

$$= -\sum_{v=1}^V \sum_i \left[ \mathbf{x}_i^v \log \check{\mathbf{x}}_i^v + (1 - \mathbf{x}_i^v) \log(1 - \check{\mathbf{x}}_i^v) \right],$$
(51)

$$\mathcal{L}'_{r} = H(\overline{\mathbf{X}}, \breve{\overline{\mathbf{X}}})$$

$$= -\sum_{i} \left[ \overline{\mathbf{x}}_{i} \log \breve{\overline{\mathbf{x}}}_{i} + (1 - \overline{\mathbf{x}}_{i}) \log(1 - \breve{\overline{\mathbf{x}}}_{i}) \right].$$
(52)

Finally, we can obtain our overall reconstruction loss  $\mathcal{L}_r$ :

$$\mathcal{L}_r = \sum_{v} \mathcal{L}_r^v + \mathcal{L}_r' \tag{53}$$

Components & Views / Datasets	ACM				Amazon Photos				
Components & views / Datasets	NMI%	ARI%	ACC%	F1%	NMI%	ARI%	ACC%	F1%	
VGMGC (w/o $\mathcal{L}_c$ )	75.0	80.6	93.1	93.1	66.1	57.1	76.4	70.4	
VGMGC (w/o $\mathcal{L}_r$ )	67.6	70.4	88.7	88.4	64.3	53.2	70.7	67.6	
VGMGC (w/o $\hat{\mathbf{S}}$ & $\mathcal{L}_E$ )	44.4	42.4	70.9	71.4	60.6	48.9	72.1	67.4	
VGMGC-single ( $\mathcal{G}^1$ )	73.1	79.6	92.8	92.8	41.9	29.5	55.1	53.5	
VGMGC-single $(\mathcal{G}^2)$	59.3	61.2	84.4	84.0	46.4	33.7	55.7	55.6	
VGMGC-original	76.3	81.9	93.6	93.6	66.8	58.4	78.5	76.9	

Table 6: The ablation study results on ACM and Amazon photos. The best results of VGMGC are shown in bold.

Methods / Datasets	) NO FEE	Co		E1 e	ND FIG	Cites		E16
	NMI%	ARI%	ACC%	F1%	NMI%	ARI%	ACC%	F1%
VGAE (Kipf and Welling 2016)	40.8	34.7	59.2	45.6	16.3	10.1	39.2	27.8
ARVGE (Pan et al. 2018)	45.0	37.4	63.8	62.7	26.1	24.5	54.4	52.9
AGC (Zhang et al. 2019)	53.7	44.8	68.9	65.6	41.1	42.0	67.0	62.3
DAEGC (Wang et al. 2019)	52.8	49.6	70.4	68.2	39.7	41.0	67.2	63.6
GMM-VGAE (Binyuan, Pengfei, and Qinghua 2020)	54.4	_	71.5	67.8	42.3	_	67.4	63.2
MAGCN (Cheng et al. 2020)	55.3	47.6	71.0	_	41.8	40.3	69.8	_
VGMGC	57.2	53.5	73.6	71.6	44.7	46.5	69.9	65.2
Methods / Datasets	BBC Sport				Three Sources			
GMC (Wang, Yang, and Liu 2020)	70.5	60.1	73.9	72.1	54.8	44.3	69.2	60.5
CGD (Tang et al. 2020)	91.0	93.1	97.4	94.7	69.5	61.1	78.1	70.9
O2MAC (Fan et al. 2020)	89.1	90.6	96.4	96.5	72.7	75.5	65.0	66.9
SDSNE (Chenghua et al. 2022)	94.8	95.8	98.5	96.8	84.8	86.7	93.5	89.8
VGMGC	96.1	96.9	98.9	99.0	85.9	87.6	94.1	92.7

Table 7: Clustering results on two single-view graph datasets (Cora and Citeseer) and two traditional multi-view datasets (BBC Sport and Three Sources). The best results are shown in bold, and the results which are not reported in the original papers are denoted by '—'.

Clustering Loss Clustering loss is specialized for clustering task (Cheng et al. 2020; Xie, Girshick, and Farhadi 2016; Xu et al. 2021a), which encourages the assignment distribution of samples in a same cluster being more similar. Concretely, let  $Q^v = \{q^v_{ij}\}$  be a soft assignment of *i*-th node to *j*-the cluster in v-th view,  $\boldsymbol{\mu}^v \in \mathbb{R}^{c \times D}$  be c centroids of c clusters,  $q^v_{ij}$  is calculated by Student's t-distribution (Maaten and Hinton 2008):

$$q_{ij}^{v} = \frac{(1 + \|\mathbf{z}_{i}^{v} - \boldsymbol{\mu}_{j}^{v}\|^{2})^{-1}}{\sum_{j} (1 + \|\mathbf{z}_{i}^{v} - \boldsymbol{\mu}_{j}^{v}\|^{2})^{-1}}.$$
 (54)

By sharpening the soft assignment  $q_{ij}^v$ , we can obtain its target distribution  $\mathbf{P}^v = \{p_{ij}^v\}$ :

$$p_{ij}^{v} = \frac{(q_{ij}^{v})^{2} / \sum_{i} q_{ij}^{v}}{\sum_{j} ((q_{ij}^{v})^{2} / \sum_{i} q_{ij}^{v})}.$$
 (55)

The clustering loss encourages soft assignment distribution  $Q^v$  to fit target distribution  $P^v$  by KL divergence, *i.e.*,  $KL(P^v\|Q^v)$ . In our multi-view clustering task, we assume that every view's soft distribution could fit the most correct target distribution, *i.e.*, the target distribution of global representation  $\overline{\mathbf{Z}}$ . Using  $\overline{P}$  and  $\overline{Q}$  denote the target and soft dis-

tribution of  $\overline{\mathbf{Z}}$ , the multi-view clustering loss could be improved as:

$$\mathcal{L}_c = \sum_{v=1}^{V} KL(\overline{P} \| Q^v) + KL(\overline{P} \| \overline{Q}).$$
 (56)

# F.4 Hyper-Parameters

Our over-smoothing analysis demonstrate that VGMGC can mitigate the issue of over-smoothing, however, the selection of order is also influenced by different datasets. In our experiments, we set order to [6, 8, 16, 16] respectively according to the dataset sizes.  $\rho$  is a soft hyper-parameter that determines the softness of beliefs of different graphs, and it is set to [0.9, 0.1, 1, 1] based on simple grid search for each dataset. For  $\gamma_c$  and  $\gamma_E$ , they are utilized to trade off the clustering loss ( $\mathcal{L}_c$ ) and ELBO ( $\mathcal{L}_E$ ), which are set to [5, 10, 5, 5] and [1, 1, 1, 1]. For the sake of adding probability to the generated consensus graph  $\hat{S}$ , we control the belief of each view by setting two hyper-parameters, i.e., maximum and minimum beliefs, as the upper and lower bounds. In the experiments, they are set to [0.99, 0.99, 0.99, 0.99]and [0.7, 0.2, 0.7, 0.7] for each dataset respectively, because some datasets may contain some unreliable graphs. Moreover, the  $\tau$  are set to 1 for all datasets. The VGMGC model

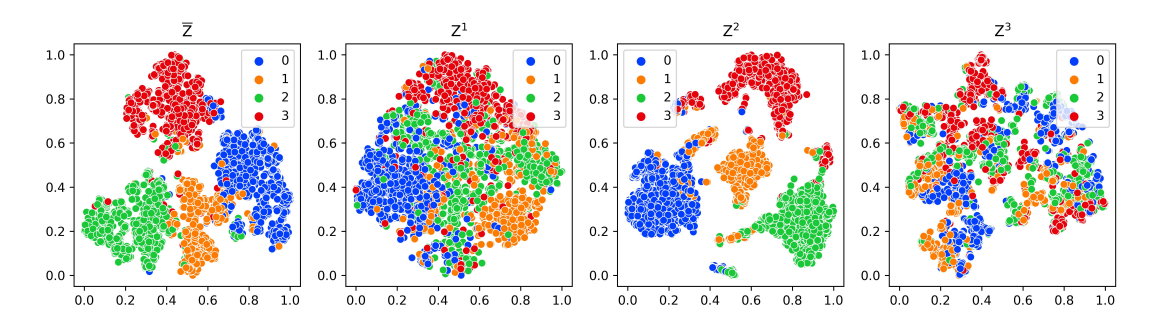


Figure 6: The visualization of t-SNE on each view's latent representation of DBLP dataset.  $\overline{\mathbf{Z}}$  denotes the multi-view fused latent representation, and the rest denote other views' representation of the dataset.

is trained for a maximum of 1000 epochs with a patience of 150 epochs, and the Adam optimizer is adopted with the learning rate of  $1\times 10^{-3}$  and weight decay of  $5\times 10^{-4}$ .

$\mathbf{A}^v$	$\mathbf{A}^v \in \mathbb{R}^{n \times n}$ represents $v$ -th view's adjacent matrix with self-loop.
$\mathbf{D}^v$	$\mathbf{D}_{ii}^v = \sum_j a_{ij}^v$ represents degree matrix of $\mathbf{A}^v$ .
$\widetilde{\mathbf{A}}^v$	$\widetilde{\mathbf{A}}^v = (\mathbf{D}^v)^{-1} \mathbf{A}^v$ represents normalized adjacent matrix.
$oldsymbol{\breve{\mathbf{A}}^v}$	The generated graph in generative process (Eq. (7)).
$\mathbf{X}^v$	$\mathbf{X}^v \in \mathbb{R}^{n \times d_v}$ represents $v$ -th view's attributed features.
$oxed{f f X}^v$	The reconstructed features to calculate $\mathcal{L}_r$ .
$\overline{\mathbf{X}}$	$\overline{\mathbf{X}} \in \mathbb{R}^{n \times d'}$ represents global features generated by concatenating all views' features.
$\overline{\mathcal{G}^v}$	$\mathcal{G}^v = (\mathbf{X}^v, \mathbf{A}^v)$ represents $v$ -th view's graph.
$\mathbf{Z}^v$	$\mathbf{Z}^v \in \mathbb{R}^{n  imes D}$ represents $v$ -th view's graph embedding.
$\overline{\overline{\mathbf{Z}}}$	$\overline{\mathbf{Z}} \in \mathbb{R}^{n \times (V \cdot D)}$ represents final global representations obtained by concatenating all $\{\mathbf{Z}^v\}$ .
$\alpha$	$oldsymbol{lpha} \in \mathbb{R}^{n \times n}$ are the neurons used to obtain $\mathbf{S}$ .
S	$\mathbf{S} = \{s_{ij} \mid s_{ij} \sim BinConcrete(\alpha_{ij}, \tau)\}$ represents the relaxed posterior probability $(q(\hat{\mathbf{S}} \mid \overline{\mathbf{X}}))$ .
ŝ	$\hat{\mathbf{S}} \in \mathbb{R}^{n \times n}$ represents the variational consensus graph.
$b^v$	$b^v$ represents belief of $v$ -th view, which can be calculated by Eq. (14).
$\beta_{ij}$	$\beta_{ij} \in (0,1]$ represents the parameter of Bernoulli distribution.
U	$U \sim Uniform(0,1)$ represents a sample from Uniform distribution between $0$ and $1$ .
$\phi'$	$\phi'$ represents the learnable parameters in $q_{\phi'}(\hat{\mathbf{S}} \mid \overline{\mathbf{X}})$ to generate $\alpha$ (Eq. (4)).
$\eta'$	$\eta'$ represents the learnable parameters in the variational approximation $q_{\eta'}(\alpha \mid \overline{\mathbf{X}})$ .
$\eta^v$	$\eta^v$ represents the learnable parameters in the variational approximation $q_{\eta^v}(\mathbf{X}^v \mid \mathbf{Z}^v)$ .
$\phi^v$	$\phi^v$ represents the learnable parameters of $f_v$ .
$\rho$	$\rho \geq 0$ is a hyper-parameter for belief $b^v$ in Eq. (14).
au	$\tau > 0$ is a hyper-parameter of temperature in Eq. (6).
order	A hyper-parameter of aggregation orders in Eq. (10).
$\mathcal{L}_c$	Task related loss for optimizing clustering results.
$\mathcal{L}_r$	Reconstruction loss for optimizing mutual information.
$\mathcal{L}_E$	Evidence lower bound for optimizing variational graph generator.
$\gamma_c$	A hyper-parameter to trade off the numerical value of $\mathcal{L}_c$ .
$\gamma_E$	A hyper-parameter to trade off the numerical value of $\mathcal{L}_E$ .

Table 8: Overall notations.